in an animal model of Pelizaeus-Merzbacher disease. J. Cell Biol. *140*, 925–934.

Griffiths, I., Klugmann, M., Anderson, T., Yool, D., Thomson, C., Schwab, M.H., Schneider, A., Zimmermann, F., McCulloch, M., Nadon, N., and Nave, K.A. (1998). Axonal swellings and degeneration in mice lacking the major proteolipid of myelin. Science *280*, 1610–1613.

Hodes, M.E., Aydanian, A., Dlouhy, S.R., Whelan, D.T., Heshka, T., and Ronen, G. (1998). A de novo mutation (C755T; Ser252Phe) in exon 6 of the proteolipid protein gene responsible for Pelizaeus-Merzbacher disease. Clin. Genet. *54*, 248–249.

Hu, B.Y., Du, Z.W., and Zhang, S.C. (2009). Differentiation of human oligodendrocytes from pluripotent stem cells. Nat. Protoc. *4*, 1614–1622.

Imaizumi, Y., Okada, Y., Akamatsu, W., Koike, M., Kuzumaki, N., Hayakawa, H., Nihira, T., Kobayashi, T., Ohyama, M., Sato, S., et al. (2012). Mitochondrial dysfunction associated with increased oxidative stress and α-synuclein accumulation in PARK2 iPSC-derived neurons and postmortem brain tissue. Mol. Brain *5*, 35.

Izrael, M., Zhang, P., Kaufman, R., Shinder, V., Ella, R., Amit, M., Itskovitz-Eldor, J., Chebath, J., and Revel, M. (2007). Human oligodendrocytes derived from embryonic stem cells: Effect of noggin on phenotypic differentiation in vitro and on myelination in vivo. Mol. Cell. Neurosci. *34*, 310–323.

Kang, S.M., Cho, M.S., Seo, H., Yoon, C.J., Oh, S.K., Choi, Y.M., and Kim, D.W. (2007). Efficient induction of oligodendrocytes from human embryonic stem cells. Stem Cells *25*, 419–424.

Lim, M.P., Devi, L.A., and Rozenfeld, R. (2011). Cannabidiol causes activated hepatic stellate cell death through a mechanism of endoplasmic reticulum stress-induced apoptosis. Cell Death Dis. *2*, e170.

Mikoshiba, K., Okano, H., Tamura, T., and Ikenaka, K. (1991). Structure and function of myelin protein genes. Annu. Rev. Neurosci. *14*, 201–217.

Nori, S., Okada, Y., Yasuda, A., Tsuji, O., Takahashi, Y., Kobayashi, Y., Fujiyoshi, K., Koike, M., Uchiyama, Y., Ikeda, E., et al. (2011). Grafted human-induced pluripotent stem-cell-derived neurospheres promote motor functional recovery after spinal cord injury in mice. Proc. Natl. Acad. Sci. USA *108*, 16825–16830.

Ohta, S., Imaizumi, Y., Okada, Y., Akamatsu, W., Kuwahara, R., Ohyama, M., Amagai, M., Matsuzaki, Y., Yamanaka, S., Okano, H., and Kawakami, Y. (2011). Generation of human melanocytes from induced pluripotent stem cells. PLoS ONE *6*, e16182.

Okada, Y., Shimazaki, T., Sobue, G., and Okano, H. (2004). Retinoic-acid-concentration-dependent acquisition of neural cell identity during in vitro differentiation of mouse embryonic stem cells. Dev. Biol. *275*, 124–142.

Okada, Y., Matsumoto, A., Shimazaki, T., Enoki, R., Koizumi, A., Ishii, S., Itoyama, Y., Sobue, G., and Okano, H. (2008). Spatiotemporal recapitulation of central nervous system development by murine embryonic stem cell-derived neural stem/progenitor cells. Stem Cells *26*, 3086–3098.

Seitelberger, F. (1995). Neuropathology and genetics of Pelizaeus-Merzbacher disease. Brain Pathol. *5*, 267–273.

Shimada, H., Okada, Y., Ibata, K., Ebise, H., Ota, S., Tomioka, I., Nomura, T., Maeda, T., Kohda, K., Yuzaki, M., et al. (2012). Efficient derivation of multipotent neural stem/progenitor cells from non-human primate embryonic stem cells. PLoS ONE *7*, e49469.

Shimojima, K., Inoue, T., Imai, Y., Arai, Y., Komoike, Y., Sugawara, M., Fujita, T., Ideguchi, H., Yasumoto, S., Kanno, H., et al. (2012). Reduced PLP1 expression in induced pluripotent stem cells derived from a Pelizaeus-Merzbacher disease patient with a partial PLP1 duplication. J. Hum. Genet. *57*, 580–586.

Southwood, C.M., Garbern, J., Jiang, W., and Gow, A. (2002). The unfolded protein response modulates disease severity in Pelizaeus-Merzbacher disease. Neuron *36*, 585–596.

Takahashi, K., Tanabe, K., Ohnuki, M., Narita, M., Ichisaka, T., Tomoda, K., and Yamanaka, S. (2007). Induction of pluripotent stem cells from adult human fibroblasts by defined factors. Cell *131*, 861–872.

Thomson, C.E., Montague, P., Jung, M., Nave, K.A., and Griffiths, I.R. (1997). Phenotypic severity of murine Plp mutants reflects in vivo and in vitro variations in transport of PLP isoproteins. Glia *20*, 322–332.

Wang, S., Bates, J., Li, X., Schanz, S., Chandler-Militello, D., Levine, C., Maherali, N., Studer, L., Hochedlinger, K., Windrem, M., and Goldman, S.A. (2013). Human iPSC-derived oligodendrocyte progenitor cells can myelinate and rescue a mouse model of congenital hypomyelination. Cell Stem Cell *12*, 252–264.

Yin, X., Baek, R.C., Kirschner, D.A., Peterson, A., Fujii, Y., Nave, K.A., Macklin, W.B., and Trapp, B.D. (2006). Evolution of a neuroprotective function of central nervous system myelin. J. Cell Biol. *172*, 469–478.

nature COMMUNICATIONS

ARTICLE

Received 12 May 2014 | Accepted 8 Oct 2014 | Published 24 Nov 2014

DOI: 10.1038/ncomms6514 OPEN

Pathological roles of the VEGF/SphK pathway in Niemann-Pick type C neurons

Hyun Lee[1,2,*], Jong Kil Lee[1,3,4,*], Min Hee Park[1,3,4], Yu Ri Hong[1,2], Hugo H. Marti[5], Hyongbum Kim[6], Yohei Okada[7], Makoto Otsu[8], Eul-Ju Seo[9], Jae-Hyung Park[10], Jae-Hoon Bae[10], Nozomu Okino[11], Xingxuan He[12], Edward H. Schuchman[12], Jae-sung Bae[1,3,4] & Hee Kyung Jin[1,2]

Sphingosine is a major storage compound in Niemann-Pick type C disease (NP-C), although the pathological role(s) of this accumulation have not been fully characterized. Here we found that sphingosine kinase (SphK) activity is reduced in NP-C patient fibroblasts and NP-C mouse Purkinje neurons (PNs) due to defective vascular endothelial growth factor (VEGF) levels. Sphingosine accumulation due to inactivation of VEGF/SphK pathway led to PNs loss via inhibition of autophagosome-lysosome fusion in NP-C mice. VEGF activates SphK by binding to VEGFR2, resulting in decreased sphingosine storage as well as improved PNs survival and clinical outcomes in NP-C cells and mice. We also show that induced pluripotent stem cell (iPSC)-derived human NP-C neurons are generated and the abnormalities caused by VEGF/SphK inactivity in these cells are corrected by replenishment of VEGF. Overall, these results reveal a pathogenic mechanism in NP-C neurons where defective SphK activity is due to impaired VEGF levels.

[1] Stem Cell Neuroplasticity Research Group, Kyungpook National University, Daegu 702-701, Korea. [2] Department of Laboratory Animal Medicine, Cell and Matrix Research Institute, College of Veterinary Medicine, Kyungpook National University, Daegu 702-701, Korea. [3] Department of Physiology, Cell and Matrix Research Institute, School of Medicine, Kyungpook National University, Daegu 700-842, Korea. [4] Department of Biomedical Science, BK21 Plus KNU Biomedical Convergence Program, Kyungpook National University, Daegu 700-842, Korea. [5] Institute of Physiology and Pathophysiology, University of Heidelberg, Heidelberg 69120, Germany. [6] Graduate School of Biomedical Science and Engineering/College of Medicine, Hanyang University, Seoul 133-791, Korea. [7] Department of Physiology, School of Medicine, Keio University, Tokyo 160-8582, Japan. [8] Division of Stem Cell Therapy, Center for Stem Cell Biology and Regenerative Medicine, Institute of Medical Science, University of Tokyo, Tokyo 108-8639, Japan. [9] Department of Laboratory Medicine, Asan Medical Center, University of Ulsan College of Medicine, Seoul 138-736, Korea. [10] Department of Physiology, School of Medicine, Keimyung University, Daegu 704-701, Korea. [11] Department of Bioscience and Biotechnology, Graduate School of Bioresource and Bioenvironmental Sciences, Kyushu University, Fukuoka 812-8581, Japan. [12] Department of Genetics and Genomic Sciences, Icahn School of Medicine at Mount Sinai, New York, New York 10029, USA. * These authors contributed equally to this work. Correspondence and requests for materials should be addressed to J.S.B. (email: jsbae@knu.ac.kr) or to H.K.J. (email: hkjin@knu.ac.kr).

Niemann–Pick type C disease (NP–C) is an inherited lipid storage disorder that affects the central nervous system[1–3]. Recent studies have shown that sphingosine is a major and initiating storage compound in NP–C[3,4]. However, the underlying mechanism(s) leading to sphingosine storage, as well as its role in NP–C pathogenesis such as neuronal loss, remains largely unknown.

Our previous studies have shown that bone marrow mesenchymal stem cells (BM-MSCs) contribute to improved neurological function in the NP–C mice[5,6]. Furthermore, we have postulated that the prosurvival effects of BM-MSCs on NP–C Purkinje neurons (PNs) are paracrine effects that restore the sphingolipid imbalance, as evidenced by decreased sphingosine and increased sphingosine-1-phosphate (S1P) levels[7]. Therefore, we speculated that sphingolipid-modulating factors derived from BM-MSCs are potential therapeutic agents for this disease.

Sphingolipid-metabolizing enzymes control the cellular dynamic balance of bioactive lipids, including the proapoptotic compound sphingosine and the proliferative compound S1P[8]. Sphingosine kinase (SphK) is a key enzyme that converts sphingosine into S1P. SphK can be activated by numerous external stimuli[9–12], resulting in a decrease in intracellular sphingosine and increase in S1P[13].

On the basis of these concepts and findings, we hypothesized that defects of SphK activators could be involved in the pathogenesis of NP–C, and explored candidate therapeutic factors secreted by BM-MSCs that might influence the activation of SphK. Here we show that NPC1 deficiency markedly reduces vascular endothelial growth factor (VEGF) expression, and that decreased VEGF levels cause impaired SphK activity in PNs. Abnormal sphingosine storage by VEGF-mediated SphK inactivity causes a decreased PN survival via disruption of autophagosome–lysosome fusion. Further, replenishment of VEGF leads to restoration of SphK activity and improvement of pathology by binding to the VEGF receptor-2 (VEGFR2) in NP–C mice PNs as well as patient-specific cells, preventing sphingosine accumulation, autophagy dysfunction and abnormal calcium homeostasis.

Results

SphK activity is reduced in NP–C patients and NP–C mice. We first determined whether defects of SphK could be involved in NP–C and responsible for the elevated sphingosine. SphK was significantly decreased in fibroblasts from NP–C patients compared with normal control fibroblasts (Fig. 1a). These levels did not change as the passage numbers increased (Fig. 1a). SphK activity also was decreased in the cerebellum and primary cerebellar PNs from NP–C mice compared with those of wild-type (WT) mice (Fig. 1a). These results confirmed that SphK, a key enzyme in modulating the levels of sphingosine, is diminished in NP–C, and that the reduction of this activity may influence disease progression and/or pathogenesis.

BM-MSC-derived VEGF restores SphK activity in NP–C mouse PNs. To examine whether bioactive, soluble factors released from BM-MSCs affected SphK activity in NP–C, we cocultured BM-MSCs with PNs using an indirect coculture system (see Methods). We found that when NP–C PNs were cocultured with BM-MSCs, their SphK activity was significantly increased (Fig. 1b). To identify the soluble factors that were released from the BM-MSCs and might be responsible for the increased SphK activity, we screened and compared the conditioned media (CM) of PNs grown with and without BM-MSCs using an antibody-based mouse cytokine array (Supplementary Fig. 1a,b). The CM of NP–C PNs cocultured with BM-MSCs revealed stronger signals in four array spots in comparison with the CM of NP–C PNs alone (Supplementary Fig. 1c,d). To confirm the secretion of these factors, we performed enzyme-linked immunosorbent assays (ELISA). Of the selected cytokines, only VEGF levels were significantly elevated in the CM of NP–C PNs cocultured with BM-MSCs. We also found that VEGF was significantly decreased in NP–C PNs cultured alone compared with WT PNs (Fig. 1c). To confirm these effects in PNs, we performed VEGF immunostaining. VEGF was normally expressed in PNs, but the expression levels were lower in NP–C PNs compared with WT PNs. When the NP–C PNs were cocultured with BM-MSCs, intensity of VEGF expression was increased (Fig. 1d). These data identified VEGF as a potential candidate molecule that could modulate SphK and may influence pathogenesis in NP–C PNs.

To further examine the effects of BM-MSC-derived VEGF on SphK activity in NP–C PNs, we used VEGF small interfering RNA (siRNA)-treated BM-MSCs and VEGF-overexpressing BM-MSCs (the latter derived from $VEGF^{tg}$ mice; ref. 14; Supplementary Fig. 2a). As predicted, SphK activity was significantly increased in NP–C PNs cocultured with BM-MSCs and $VEGF^{tg}$ BM-MSCs compared with NP–C PNs alone. However, the activity did not show any changes in NP–C PNs cocultured with VEGF siRNA-treated BM-MSCs (Fig. 1e). Consistent with this observation, sphingosine and S1P levels in the cocultured NP–C PNs were altered relative to the amount of VEGF released from the BM-MSCs (Supplementary Fig. 2b,c). We also performed S1P immunostaining in PNs. S1P was mainly expressed in PNs, and the expression was significantly increased in NP–C PNs cocultured with normal or $VEGF^{tg}$ BM-MSCs. However, it was not increased when the cells were cocultured with VEGF siRNA-treated BM-MSCs (Supplementary Fig. 2d).

VEGF binds to two tyrosine kinase receptors, known as VEGFR1 and 2 (ref. 15). Among these receptors, VEGFR2 is highly expressed on PNs[16]. To examine whether VEGF from BM-MSCs improved the sphingolipid imbalance in NP–C PNs by binding to VEGFR2, we treated NP–C PNs with the VEGFR2 tyrosine kinase inhibitor PTK787 before coculturing[17]. We found that SphK activity and other sphingolipid metabolites in NP–C PNs were mediated by interactions of BM-MSC-derived VEGF and its receptor VEGFR2 (Fig. 1f; Supplementary Fig. 2e). These results indicated that BM-MSC-mediated restoration of abnormal SphK activity could be due the secreted VEGF binding to the VEGFR2 in NP–C PNs.

Next, to determine whether the VEGF-mediated SphK modulation by BM-MSCs promoted the survival of NP–C PNs, we determined cell counts after coculture. When NP–C PNs were cocultured with BM-MSCs or $VEGF^{tg}$ BM-MSCs, the number of PNs was significantly increased. This effect was lower when VEGF siRNA BM-MSCs were cocultured with the NP–C PNs, although this did not reach statistical significance (Fig. 1g).

Finally, to gain more direct insights into the relationship between VEGF and SphK activity in NP–C PNs, we treated WT PNs with VEGF siRNA and determined the changes of sphingolipid factors. VEGF siRNA treatment of WT PNs strongly reduced SphK levels and led to elevation of sphingosine and reduction of S1P, similar to NP–C PNs (Fig. 1h; Supplementary Fig. 2f,g). The survival of PNs was also significantly decreased following VEGF siRNA transfection (Fig. 1i). These results suggested that inactivation of VEGF may lead to reduced SphK activity in NP–C PNs.

VEGF from BM-MSCs reduces pathology in PNs of NP–C mice. To examine the *in vivo* effects of VEGF derived from BM-MSCs on SphK activity of PNs, we transplanted BM-MSCs into the cerebellum of NP–C mice (Fig. 2a). At one day after BM-MSC

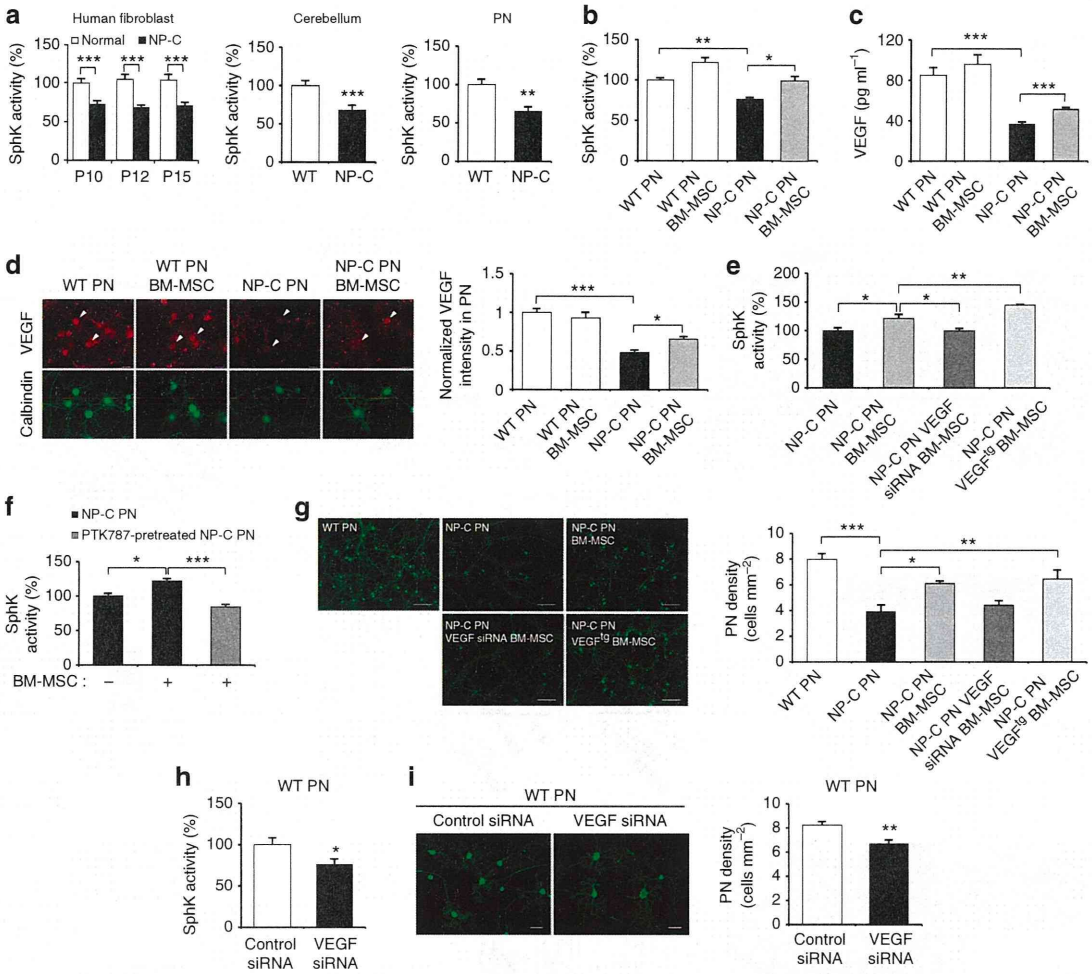

Figure 1 | BM-MSC-derived VEGF restores SphK activity in NP-C mice PNs. (**a**) SphK activities between NP-C and control were analysed in human fibroblast ($n=7$ per group), mouse cerebellum tissue ($n=7$ per group) and primary mouse PN samples ($n=9$ per group). SphK activity did not show passage differences between NP-C and normal fibroblasts. (**b**) Three days after cocultures, we measured SphK activities in PNs derived from WT and NP-C mice ($n=8$ per group). (**c**) VEGF levels were measured in CM derived from PNs with or without BM-MSCs by ELISA ($n=7$ per group). (**d**) Primary cultures of NP-C PNs were immunostained with anti-calbindin and anti-VEGF (scale bar, 50 μm). Arrowheads indicate VEGF expression by PNs. Values represent normalized fluorescence intensities of VEGF in PNs (WT PN, $n=8$; and NP-C PN, $n=9$). (**e**) SphK activities were measured in NP-C PNs alone ($n=7$) and NP-C PNs cocultured with BM-MSCs, VEGF siRNA BM-MSCs and $VEGF^{tg}$ BM-MSCs ($n=8$ per group). (**f**) Effect of the PTK787 on BM-MSCs mediated SphK activation. NP-C PNs were pretreated with PTK787 at 10 μM for 1 day and cocultured for 3 days with BM-MSCs, and then SphK activity was assayed ($n=7$ per group). (**g**) Representative images of PNs stained with anti-calbindin (scale bar, 100 μm). The mean number of PNs per squared millimetre was counted ($n=8$ per group). (**h**) Effect of VEGF knockdown on SphK activity in PNs (control, $n=6$; and VEGF siRNA, $n=8$ per group). (**i**) Representative images and quantification of neuronal survival in normal and VEGF-knockdown PNs (scale bar, 50 μm; $n=8$ per group). **a**,**h**,**i**, Student's *t*-test. **b**–**g**, one-way analysis of variance, Tukey's *post hoc* test. $^*P<0.05$, $^{**}P<0.01$, $^{***}P<0.005$. All error bars indicate s.e.m.

transplantation, SphK activity was significantly increased in the cerebellum of NP–C mice compared with phosphate-buffered saline (PBS)-infused counterparts (Fig. 2b). BM-MSC transplantation also increased VEGF protein levels in the cerebellum of NP–C mice (Fig. 2c). The elevated expression of VEGF was significant in the Purkinje cell layer (PCL) of the NP–C mouse cerebellums, consistent with the decreased VEGF levels in non-treated NP–C PNs compared with WT (Fig. 2d). However, BM-MSCs did not increase SphK or VEGF levels in normal cerebellums, consistent with previous reports[6,18].

We also transplanted VEGF siRNA BM-MSCs and $VEGF^{tg}$ BM-MSCs into the cerebellum of NP–C mice. As predicted, at one day after transplantation, SphK activity was significantly increased in the cerebellum of NP–C mice treated with $VEGF^{tg}$ BM-MSCs. However, mice treated with VEGF siRNA BM-MSCs showed significantly lower SphK activity (Fig. 2e). The sphingosine and S1P metabolites were also changed in NP–C PNs in relation to SphK and VEGF levels (Supplementary Fig. 3a,b). Similar effects were observed when S1P immunostaining was performed on the PN layer of NP–C mice following transplantation with VEGF siRNA or VEGF-overexpressing BM-MSCs (Supplementary Fig. 3c). To further confirm these effects, we used laser capture microdissection (LCM) to selectively isolate PNs (Supplementary Fig. 3d). We observed that expressions of *Vegf*, *VEGFR2* and *Sphk1* mRNAs were decreased in LCM-captured PNs from NP–C mice compared with that of WT mice. BM-MSC transplantation enhanced these expression levels in NP–C PNs (Fig. 2f). We also ascertained whether VEGFR2 was required for the activation of SphK in NP–C mice. As shown in Fig. 2g, SphK activity was significantly increased in the NP–C mice following BM-MSC treatment, whereas this effect was lower in NP–C mice treated with PTK787 before injecting BM-MSCs,

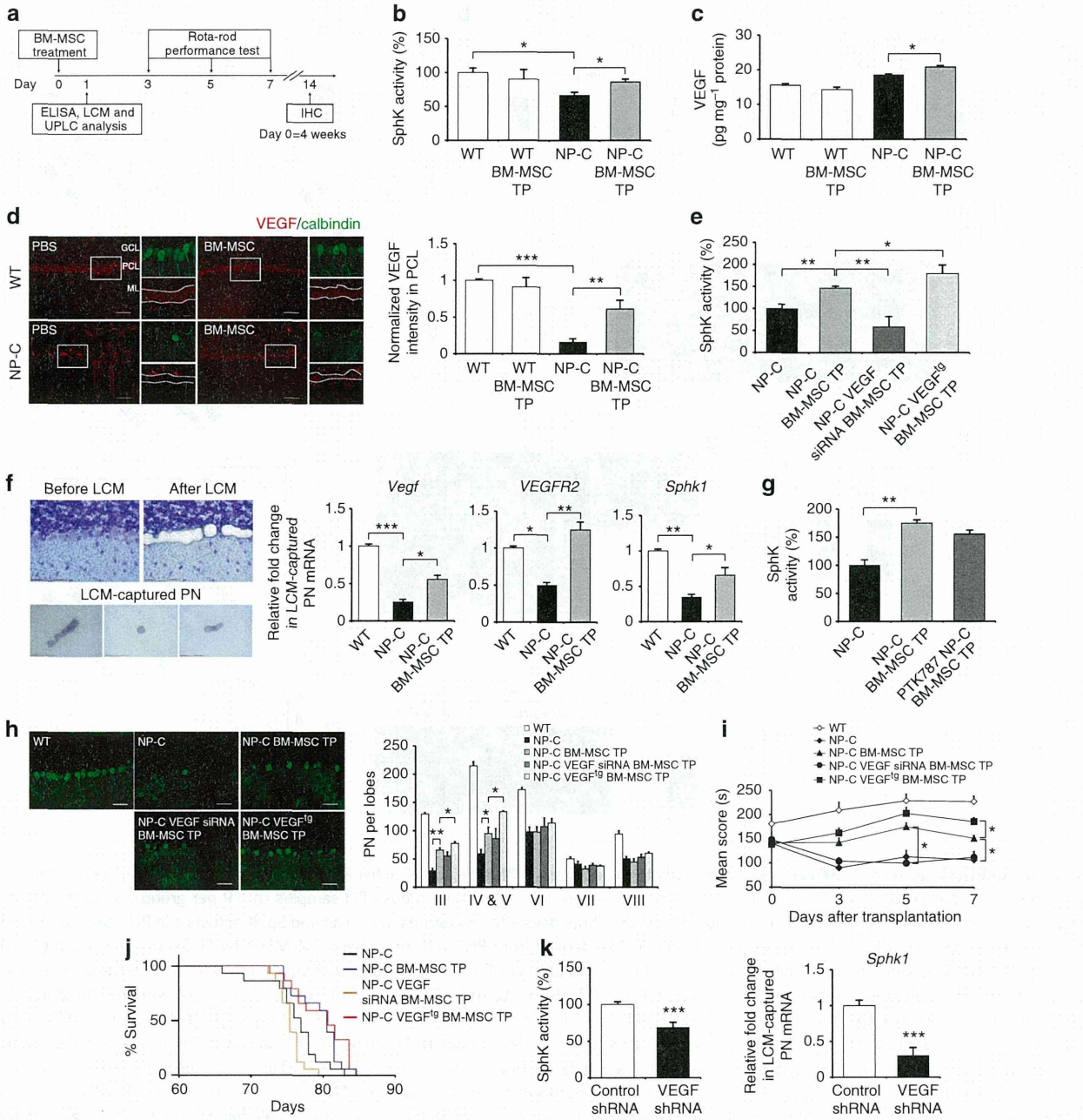

Figure 2 | VEGF from BM-MSCs reduces pathology in PNs of NP-C mice. (**a**) Protocol of BM-MSC treatment in NP-C mice. (**b**,**c**) SphK activity ($n=7$ per group; **b**) and VEGF levels ($n=8$ per group; **c**) were estimated in the cerebellums of WT and NP-C mice after BM-MSC treatment. (**d**) Cerebellar sections were stained with anti-calbindin and anti-VEGF (low-magnification scale bar, 50 μm; high-magnification scale bar, 20 μm). Values represent normalized VEGF fluorescence intensities in PCL ($n=7$ per group). (**e**) SphK activities were measured in the cerebellums of NP-C mice treated with PBS ($n=6$), BM-MSCs, VEGF siRNA BM-MSCs and $VEGF^{tg}$ BM-MSCs ($n=8$ per group). (**f**) Left, isolation of mouse PNs using LCM (scale bar, 75 μm). Right, mRNA level of *Vegf*, *VEGFR2* and *Sphk1* on LCM-captured PNs samples ($n=7$ per group). (**g**) NP-C mice were treated daily with the PTK787 at 100 mg kg^{-1} or PBS, starting 2 days before the BM-MSC transplantation. One day after BM-MSC treatment, SphK activity was estimated (NP-C, $n=7$; NP-C BM-MSC TP, $n=8$ per group). (**h**) Cerebellar sections were stained with anti-calbindin (scale bar, 50 μm), and the number of calbindin-positive PNs were quantified ($n=7$ per group). (**i**) Rota-rod scores of mice were averaged and plotted beginning 3 days after transplantation ($n=15$ per group). (**j**) Survival curve of NP-C mice ($n=15$ per group). Treatment with BM-MSCs and $VEGF^{tg}$ BM-MSCs resulted in significantly increased survival compared with PBS treatment ($P=0.0194$ and $P=0.0055$, respectively; log-rank test). (**k**) Effect of VEGF knockdown on SphK activity. Left, after intracerebellar injection of control ($n=7$) or VEGF shRNA ($n=8$) in mice, SphK activities were measured in the cerebellums. Right, relative levels of *Sphk1* mRNA from LCM-captured PNs samples ($n=7$ per group). **b**–**i**, one-way analysis of variance, Tukey's *post hoc* test. **k**, Student's *t*-test. $^{*}P<0.05$, $^{**}P<0.01$, $^{***}P<0.005$. All error bars indicate s.e.m.

although this did not reach statistical significance. S1P levels were moderately decreased with PTK787 treatment, but sphingosine did not vary between the groups (Supplementary Fig. 3e).

Next, we evaluated the effects of VEGF on the NP-C phenotype in mice. Transplantation of $VEGF^{tg}$ BM-MSCs improved NP-C pathology as measured by increased number

of calbindin-positive PNs on 14 days after treatment (Fig. 2h), and also enhanced the Rota-rod performance (Fig. 2i). These effects were less in the VEGF siRNA BM-MSC-treated group. Rota-rod performance also diminished in the VEGF siRNA BM-MSC-treated NP–C mice over time. Moreover, the lifespan of mice that had BM-MSC or VEGF^{tg} BM-MSC transplants was extended (Fig. 2j).

Finally, to determine whether the reduced VEGF levels in the cerebellums affected SphK activity, we injected VEGF short hairpin RNA (shRNA) into the cerebellum of WT mice and determined the changes of sphingolipid factors. Treatment with VEGF shRNA markedly reduced SphK activity and *Sphk1* mRNA levels (Fig. 2k; Supplementary Fig. 3f,g) and led to elevation of sphingosine and reduction of S1P (Supplementary Fig. 3h). These results suggested that inactivation of VEGF may lead to reduced SphK activity in NP–C mice, consistent with *in vitro* results. Together, these findings show a direct correlation between VEGF and SphK activity in PNs and suggest that abnormal sphingosine accumulation in NP–C may be due to the dysfunction of SphK activity by inactivated VEGF expression.

NPC1 deficiency impairs VEGF/SphK activation in PNs. We subsequently investigated the relationship between NPC1 and VEGF expression. NPC1 knockdown by siRNA markedly decreased VEGF expression in normal PNs. When NPC1 was knocked down in VEGF^{tg} PNs (derived from VEGF^{tg} mice), the decreased level of VEGF was lower than that of normal PNs (Fig. 3a–c). Moreover, NPC1 deficiency markedly inactivated SphK and led to sphingolipid imbalance. In VEGF^{tg} PNs, however, moderate changes were observed (Fig. 3d,e). We next tested whether NPC1 deficiency affected VEGF expression in the

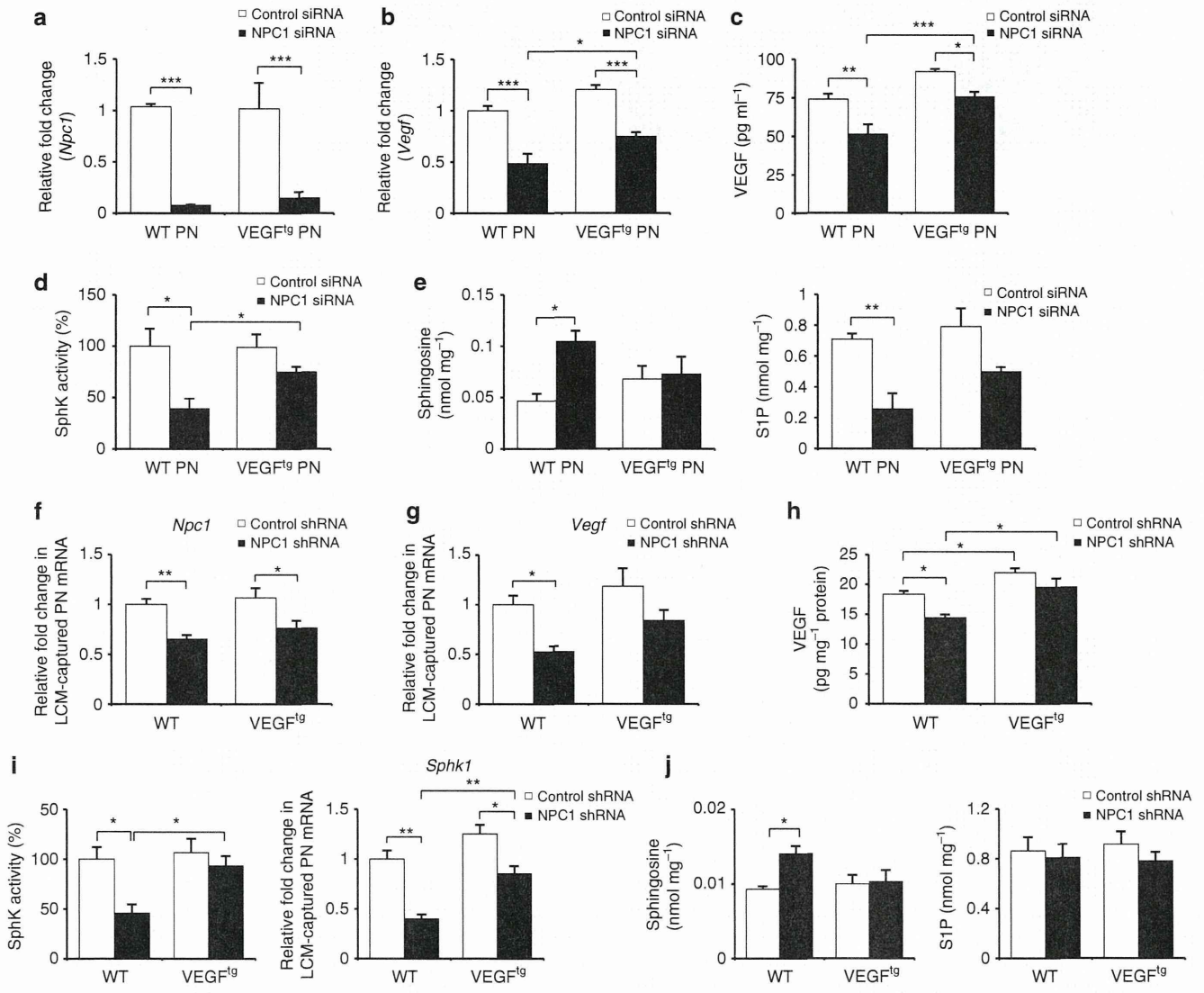

Figure 3 | NPC1 knockdown reduces VEGF expression and SphK activity. (**a**–**c**) Primary cultures of normal and VEGF^{tg} PNs were transfected with control or NPC1 siRNA. Three days after transfection, we measured the levels of *Npc1* (**a**) and *Vegf* (**b**) mRNA and secreted VEGF protein (**c**) in PNs ($n=7$ per group). (**d**,**e**) SphK activity (**d**), sphingosine and S1P (**e**) were estimated in PNs transfected with control ($n=6$) or NPC1 siRNA ($n=7$). (**f**–**j**) Four-week-old WT and VEGF^{tg} mice were injected with control or NPC1 shRNA into the cerebellum. Mice were sacrificed at 3 days after the injection. *Npc1* (**f**) and *Vegf* (**g**) mRNA levels were estimated in LCM-captured PNs and VEGF protein levels (**h**) were measured in the cerebellums ($n=7$ per group). (**i**) Left, SphK activities were measured in the cerebellums ($n=7$ per group). Right, relative levels of *Sphk1* mRNA from LCM-captured PNs samples ($n=8$ per group). (**j**) Sphingosine and S1P were measured in the cerebellums ($n=7$ per group). **a**–**j**, one-way analysis of variance, Tukey's *post hoc* test. $^*P<0.05$, $^{**}P<0.01$, $^{***}P<0.005$. All error bars indicate s.e.m.

cerebellums of WT mice using NPC1 shRNA. Intracerebellar injection of NPC1 shRNA, which decreased *Npc1* mRNA expression in the LCM-captured PNs (Fig. 3f), reduced VEGF expression (Fig. 3g,h). Consistently, NPC1 deficiency significantly decreased SphK activity and *Sphk1* mRNA expression and led to elevation of sphingosine and reduction of S1P in the cerebellums (Fig. 3i,j). These effects were moderated in VEGF^{tg} mice (Fig. 3g–j). Overall, these results indicated that knockdown of NPC1 may lead to reduced VEGF expression, and these reductions subsequently decreased SphK activity in PNs.

VEGF overexpression ameliorates NP-C pathology in mice. The VEGF-mediated SphK reduction in NP-C PNs prompted us to examine possible genetic implications of this pathway. To increase VEGF in NP-C mice, we generated *VEGF^{tg}/Npc1$^{-/-}$* mice (Supplementary Fig. 4a). VEGF is widely expressed in neurons, glia and endothelial cells[19,20], with strong expression in PNs. In NP-C cerebellum, however, VEGF was mainly expressed in the granular layer and significantly decreased in the PCL. VEGF/NP-C mice showed increased expression of VEGF in the PCL compared with NP-C mice (Fig. 4a).

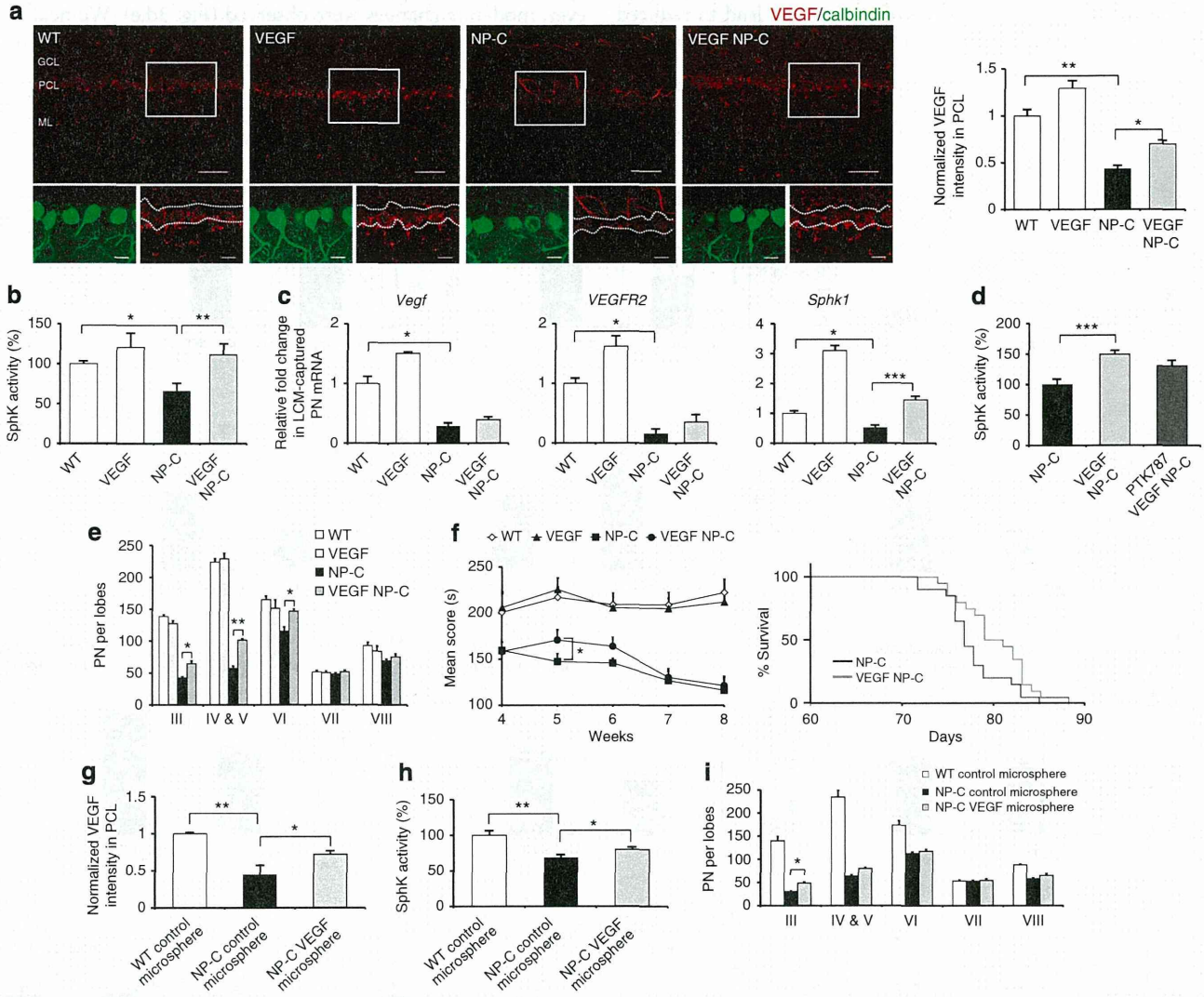

Figure 4 | Replenishment of VEGF ameliorates NP-C pathology in mice. (**a**) Cerebellar sections from 6-week-old WT, VEGF, NP-C and VEGF/NP-C mice were immunostained with anti-calbindin and anti-VEGF (low-magnification scale bar, 50 μm; high-magnification scale bar, 20 μm). The average VEGF fluorescence intensity within the PCL was measured (WT, $n=7$; VEGF, $n=7$; NP-C, $n=9$; and VEGF/NP-C, $n=9$). (**b**) SphK activities were measured in cerebellums derived from 6-week-old WT, VEGF, NP-C and VEGF/NP-C mice ($n=8$ per group). (**c**) Quantitative real-time PCR for *Vegf*, *VEGFR2* and *Sphk1* mRNA in LCM-captured PNs in 6-week-old WT, VEGF, NP-C and VEGF/NP-C mice (WT, $n=6$; VEGF, $n=6$; NP-C, $n=8$; and VEGF/NP-C, $n=8$). (**d**) VEGF/NP-C mice were treated daily with the PTK787 at 100 mg kg^{-1} or PBS vehicle control for 3 days before sacrifice (6-week-old), and SphK activity was estimated in cerebellums ($n=7$ per group). (**e**) Cerebellar sections were immunostained with anti-calbindin and the number of calbindin-positive PNs was quantified (WT, $n=7$; VEGF, $n=7$; NP-C, $n=8$; and VEGF/NP-C, $n=8$). (**f**) Left, beginning at 4 weeks of age, Rota-rod scores were averaged and plotted ($n=15$ per group). Right, survival curves of NP-C and VEGF/NP-C mice ($P=0.0548$; log-rank test, $n=15$ per group). (**g**) Cerebellar sections from WT and NP-C mice transplanted with VEGF-loaded or control microspheres were stained with anti-calbindin and anti-VEGF. The average VEGF fluorescence intensity within the PCL was measured ($n=7$ per group). (**h**) SphK activity was estimated in the cerebellums of WT and NP-C mice at one day after treatment. (**i**) Cerebellar sections were prepared at 2 weeks after transplantation and immunostained with anti-calbindin. The calbindin-positive PNs were counted ($n=7$ per group). **a–i**, one-way analysis of variance, Tukey's *post hoc* test. $^*P<0.05$, $^{**}P<0.01$, $^{***}P<0.005$. All error bars indicate s.e.m.

To examine whether genetically increasing VEGF affects SphK activity in NP–C PNs, we analysed cerebellum samples derived from 6-week-old WT, VEGF, NP–C and VEGF/NP–C mice. Compared with NP–C mice, VEGF/NP–C mice showed significantly increased SphK activity and decreased sphingosine accumulation (Fig. 4b; Supplementary Fig. 4b). Cerebellar S1P levels did not vary between the NP–C and VEGF/NP–C mice, although S1P levels in the PCL was increased in VEGF/NP–C mice (Supplementary Fig. 4b,d). Sphingomyelin and unesterified cholesterol levels were also significantly decreased in VEGF/NP–C mice, but glycosphingolipid (GSL) levels did not vary between the groups (Supplementary Fig. 4c,e,f). These results revealed that genetic VEGF overexpression could reverse the SphK abnormality and abnormal lipid accumulation in NP–C. To confirm VEGF-mediated SphK activation within PNs, we measured the *Vegf*, *VEGFR2* and *Sphk1* mRNA levels in LCM-captured PNs from these mice. LCM-captured PNs from VEGF/NP–C showed slightly increased *Vegf* and *VEGFR2* mRNA levels and significantly enhanced *Sphk1* mRNA levels (Fig. 4c).

Next, to further investigate the subcellular distribution pattern of SphK activity, sphingosine and S1P, we isolated cytosolic-enriched and lysosome-enriched fractions from the cerebellums. SphK activity was increased in VEGF/NP–C-derived lysosomes and cytosol compared with NP–C-derived ones, although the degree of SphK increase was greater in the cytosol than lysosome. Accumulated sphingosine in NP–C was found in the lysosome. Lysosomal sphingosine levels were significantly decreased in the VEGF/NP–C, whereas S1P levels did not vary between the groups (Supplementary Fig. 4g). Taken together, these results suggested that VEGF leads to activated SphK in the lysosome and cytosol and that activated SphK decreased lysosomal sphingosine accumulation in NP–C. We next observed whether the activation of VEGFR2 was required for the activation of SphK in VEGF/NP–C mice. Increased SphK activity was lower in VEGF/NP–C mice treated with the PTK787, although this did not reach statistical significance (Fig. 4d). Sphingosine levels also were moderately increased, but S1P levels did not vary between the groups (Supplementary Fig. 4h). PN survival was significantly improved in the VEGF/NP–C mice (Fig. 4e), and there were improvements in the Rota-rod score of 5-week-old VEGF/NP–C mice compared with NP–C mice (Fig. 4f, left). The lifespan of the VEGF/NP–C mice was slightly increased (Fig. 4f, right). We also found that BM-MSC transplantation is more effective in SphK modulation than genetic replenishment of VEGF (see Fig. 2). These results suggested that other factors secreted by BM-MSCs might also contribute to SphK activation.

We next tested whether pharmacologic delivery of recombinant VEGF is beneficial to NP–C pathology. Since the injected recombinant VEGF exerted a short-lived effect[21], to overcome this obstacle we generated a microsphere system that allows localized and sustained VEGF release (Supplementary Fig. 5a). We injected 3 mg of VEGF-loaded microspheres or control microspheres into the cerebellum of 4-week-old NP–C and WT mice. Two weeks after treatment, NP–C mice transplanted with VEGF-loaded microspheres had higher levels of VEGF expression in the PCLs (Fig. 4g), exhibited increased SphK activity (Fig. 4h) and decreased sphingosine levels (Supplementary Fig. 5b) in their cerebellums. S1P levels in cerebellum and expression in PNs were also increased by VEGF-loaded microsphere treatment (Supplementary Fig. 5b,c). Further, the VEGF-loaded microsphere-treated NP–C mice showed significantly improved PN survival (Fig. 4i).

VEGF overexpression reverses defective autophagy in NP–C mice. Autophagy, a major degradative pathway of the lysosomal system, is known to be markedly impaired in NP–C. These defects lead to loss of PNs in NP–C[22]. To examine whether increased PN survival in VEGF/NP–C mice was related to autophagy, we first measured LC3-II levels. Consistent with previous result[22], we found that the LC3-II levels were significantly increased in PNs and cerebellum samples derived from NP–C mice. This enhanced LC3-II level was reduced in VEGF/NP–C mice (Fig. 5a,b,d). The level of beclin-1 did not vary between the groups (Fig. 5a,d). The levels of cathepsin D, a lysosomal hydrolase, were slightly increased in NP–C mice compared with WT mice (Fig. 5a,d). However, the activity of cathepsin D was not changed between the groups (Fig. 5c,e). This result indicated that the elevated levels of cathepsin D in NP–C mice did not ultimately translate into a significant increase in enzyme activity. Cathepsin D levels in VEGF/NP–C mice were comparable to that of NP–C mice, indicating that increased VEGF in NP–C mice did not influence the cathepsin D expression (Fig. 5a,c–e). The level of p62 was significantly higher in NP–C mice compared with WT mice, but was decreased in VEGF/NP–C mice (Fig. 5a,d). We also performed transmission electron microscopic (EM) analysis using mouse cerebellum samples to corroborate the immunoblotting results. NP–C mice brains showed massive increases of autophagic vacuoles, while brains of VEGF/NP–C mice represented a reduced number of these vesicles (Fig. 5f).

Next, to determine whether the endocytic pathway was affected by VEGF overexpression in NP–C mice, we examined Rab5 and Rab7 expression in our animals. The levels of these proteins showed no differences between the groups (Fig. 5g). Apoptotic cells, as judged by active caspase-3, did not show any differences between NP–C and VEGF/NP–C mice (Fig. 5h). Our results showed that endocytic pathway and apoptosis were not the main mechanisms of increased PN survival in VEGF/NP–C mice.

Impaired VEGF/SphK pathway causes defective autophagic flux. Improved autophagic degradation in the VEGF/NP–C mice prompted us to analyze whether VEGF-mediated sphingolipid changes affect autophagy activity. First, to unravel the mechanistic link between VEGF levels and autophagic dysfunction, VEGF was depleted in the WT PNs by siRNA treatment. Knockdown of VEGF caused increased accumulation of LC3-II and p62 (Fig. 6a,b). Beclin-1 expression was not affected by VEGF knockdown (Fig. 6a), indicating that the accumulation of autophagosomes was not due to the biogenesis pathway.

The accumulation of autophagosomes can occur due to either an increase in their rate of formation or a reduction in their rate of degradation[23]. To distinguish between these two events, we examined the effects of VEGF knockdown on LC3-II levels in WT PNs in the presence or absence of NH_4Cl that blocks autophagic degradation but does not affect autophagosome formation. VEGF knockdown increased accumulation of LC3-II. This level was not further increased by NH_4Cl treatment (Fig. 6c, left). In contrast, VEGF depletion in serum starvation culture resulted in a significant increase in LC3-II levels (Fig. 6c, right). These observations were also supported by levels of p62 (Fig. 6c). These results suggested that VEGF depletion influences at a late step of autophagy. We also performed autophagy flux assay in WT, NP–C and VEGF/NP–C mice PNs. Under basal condition, NP–C PNs showed significantly increased LC3-II and p62 levels compared with WT PNs. NH_4Cl-induced lysosome inhibition led to marked increase of LC3-II and p62 levels in the WT PNs, but this increase was significantly less in the NP–C PNs (Fig. 6d). VEGF/NP–C PNs showed similar pattern in LC3-II and p62 increase compared with WT cells (Fig. 6d). Taken together, these

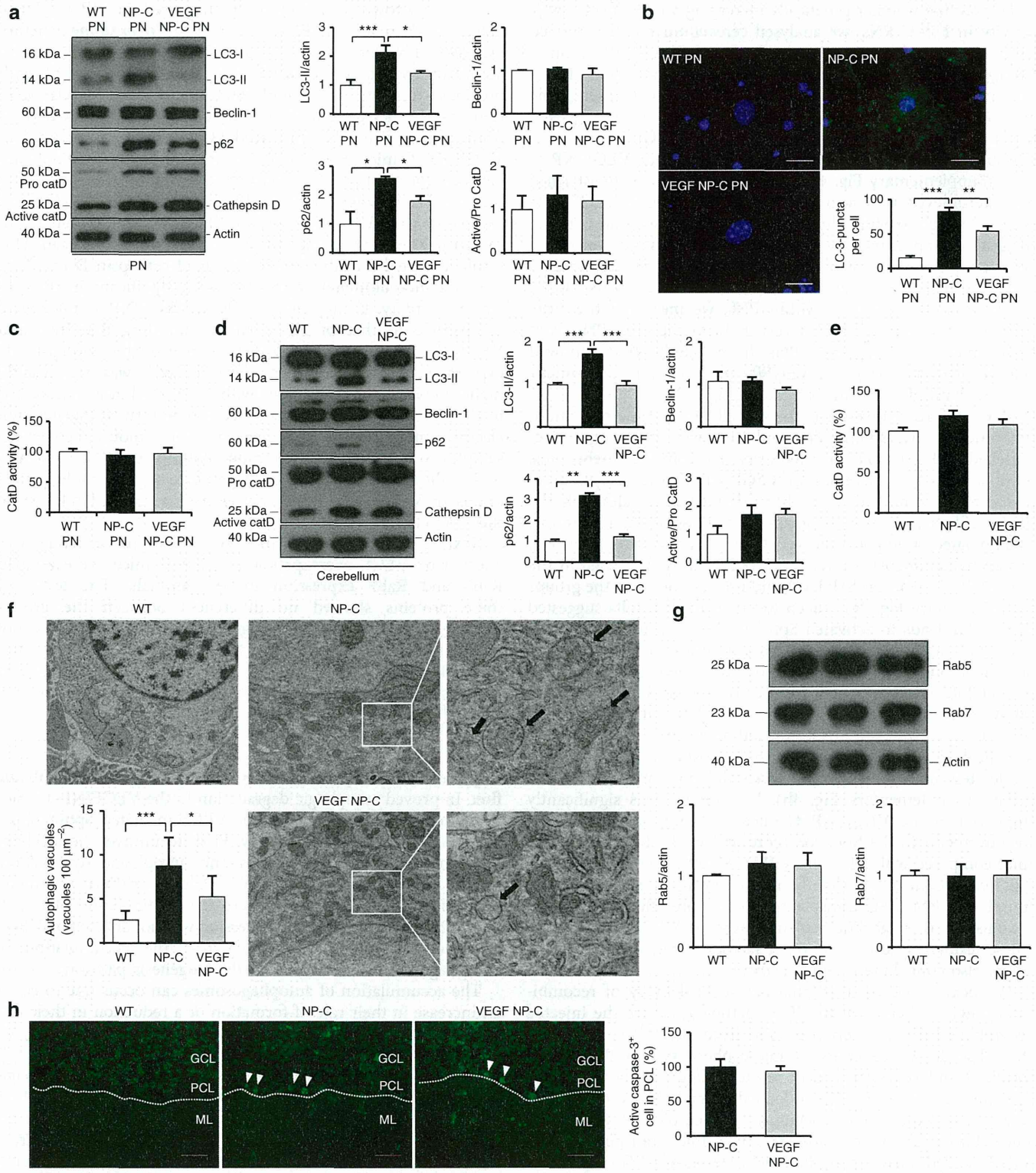

Figure 5 | VEGF replenishment reverses defective autophagy in NP-C mice. (**a**) Western blot analysis of LC3, beclin-1, p62 and cathepsin D in primary cultured PNs derived from WT, NP-C and VEGF/NP-C mice (WT, $n=5$; NP-C, $n=6$; and VEGF/NP-C, $n=6$). (**b**) Immunocytochemistry of LC3 in WT, NP-C and VEGF/NP-C PNs ($n=6$ per group; scale bar, 20 μm). (**c**) Cathepsin D activity in primary cultured PNs (WT, $n=5$; NP-C, $n=6$; and VEGF/NP-C, $n=6$). (**d**) Western blot analysis of LC3, beclin-1, p62 and cathepsin D in the cerebellums of 6-week-old WT, NP-C and VEGF/NP-C mice (WT, $n=6$; NP-C, $n=7$; and VEGF/NP-C, $n=7$). (**e**) Cathepsin D activity in the cerebellums of WT, NP-C and VEGF/NP-C mice (WT, $n=5$; NP-C, $n=6$; and VEGF/NP-C, $n=6$). (**f**) EM images and quantification data of the cerebellum ($n=5$ per group; low-magnification scale bar, 1 μm; high-magnification scale bar, 200 nm). Arrow indicates autophagic vacuole. (**g**) Western blot analysis of Rab5 and Rab7 levels in the cerebellum ($n=6$ per group). (**h**) Cerebellar sections were immunostained with anti-active caspase-3 and the number of active caspase-3-positive cells in PCL was quantified ($n=5$ per group; scale bar, 50 μm). **a**–**g**, one-way analysis of variance, Tukey's *post hoc* test. **h**, Student's *t*-test. $^*P<0.05$, $^{**}P<0.01$, $^{***}P<0.005$. All error bars indicate s.e.m.

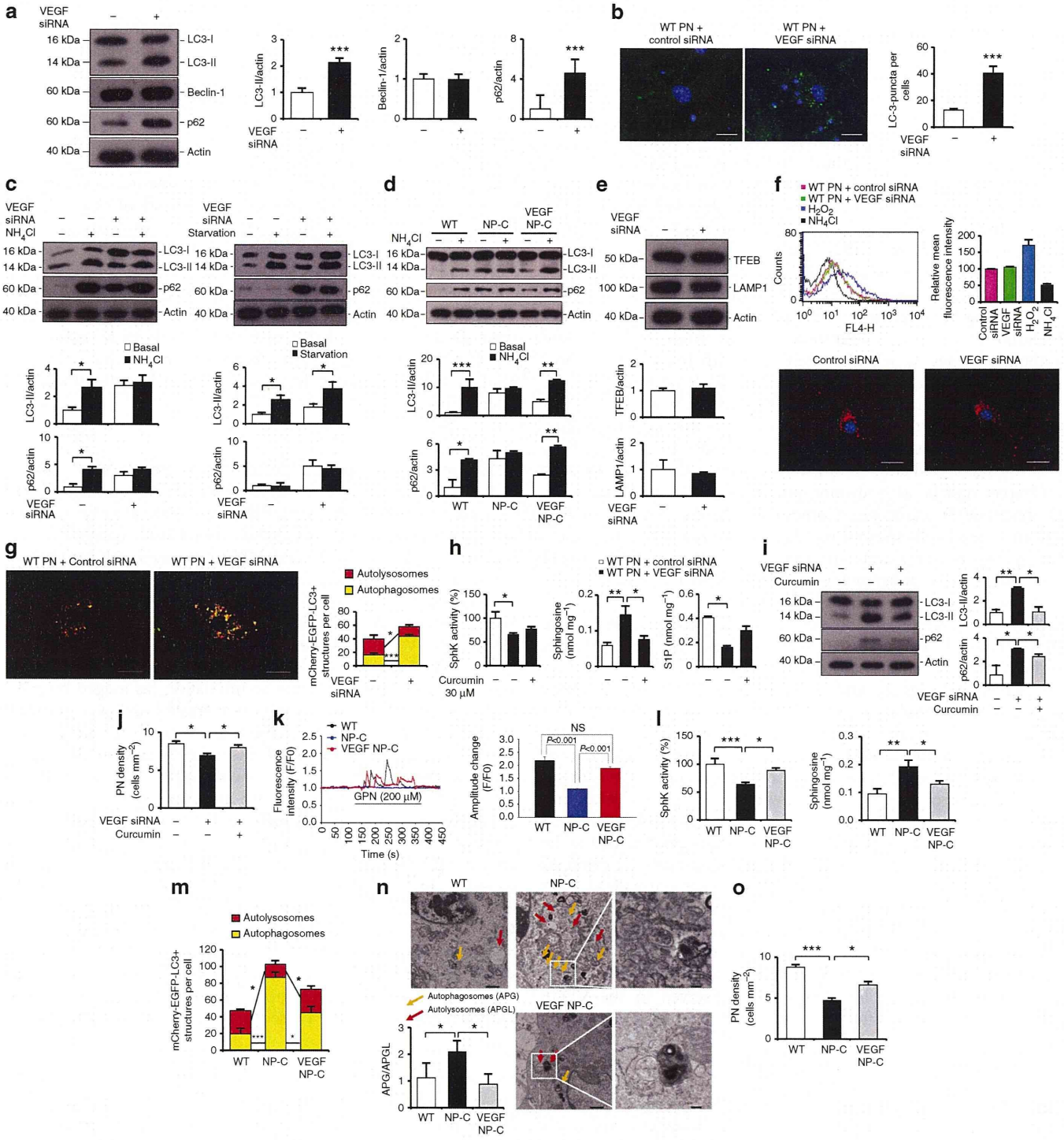

Figure 6 | VEGF/SphK inactivity impairs autophagic flux. (**a**) Western blots of LC3, beclin-1 and p62 in PNs after VEGF knockdown ($n=6$ per group). (**b**) Immunocytochemistry of LC3 in PNs after VEGF knockdown ($n=6$ per group; scale bar, 20 μm). (**c**) Autophagic flux assay. Western blots of LC3 and p62 in PNs ($n=6$ per group). (**d**) Western blots of LC3 and p62 in cultured PNs in the presence of NH_4Cl ($n=5$ per group). (**e**) Western blots of TFEB and Lamp1 in VEGF-knockdown PNs (control, $n=5$ and VEGF siRNA, $n=6$). (**f**) Effect of VEGF knockdown on lysosomal pH. PNs stained with LysoTracker red ($n=5$ per group; scale bar, 20 μm). (**g**) Fluorescence analysis of autophagosomes and autolysosomes (control, $n=7$ and VEGF siRNA, $n=8$; scale bar, 10 μm). (**h**) Sphk activity, sphingosine and S1P levels in PNs after VEGF knockdown in the presence of curcumin ($n=8$ per group). (**i**) Western blot analysis of LC3 and p62 in VEGF-knockdown PNs treated with curcumin (control, $n=7$; VEGF siRNA, $n=8$; and VEGF siRNA/curcumin, $n=8$). (**j**) Survival of VEGF-knockdown PNs treated with curcumin ($n=8$ per group). (**k**) Left, representative traces showing intracellular [Ca^{2+}] changes monitored in single fluo-4-loaded PNs. Right, maximal peak fluorescence changes were determined as the differences between basal and the maximum fluorescence ($n=10$ cells per group). (**l**) Sphk activity and sphingosine levels were measured in cultured PNs ($n=8$ per group). (**m**) Quantification of autophagosomes and autolysosomes in primary cultured PNs (WT, $n=7$; NP-C, $n=7$; and VEGF/NP-C, $n=8$). (**n**) EM analysis of the PNs ($n=5$ per group; low-magnification scale bar, 1 μm; high-magnification scale bar, 200 nm). (**o**) Survival of primary cultured PNs (WT, $n=6$; NP-C, $n=8$; and VEGF/NP-C, $n=8$). **a**,**b**,**e**,**g**, Student's *t*-test. **c**,**d**,**f**,**h**–**o**, one-way analysis of variance, Tukey's *post hoc* test. $^*P<0.05$, $^{**}P<0.01$, $^{***}P<0.005$. All error bars indicate s.e.m.